ACS Partner Journal

CHEM & BIO ENGINEERING

pubs.acs.org/ChemBioEng

Article

Development of Shaped MIL-100(Fe) Granules for High-Performing Adsorption Desalination: From Formulation Optimization to System Test

Hao Chen, Qiancan Wang, Long Chen, Shanshan Cai, Jing Lei, and Song Li*

Cite This: *Chem Bio Eng.* 2024, 1, 817−825

Read Online

ACCESS | Metrics & More | Article Recommendations | Supporting Information

ABSTRACT: Adsorption desalination (AD) driven by low-grade renewable energy or waste heat is a sustainable solution to the water crisis. Recently, metal−organic frameworks (MOFs) with excellent water adsorption performances have been recognized as some of the most promising candidates for AD. However, previous studies mainly focused on MOFs in powder form, causing pipe clogging and a drastic pressure drop, which inspire the development of shaped MOFs for industrial use. In this work, MIL-100(Fe) with high water stability, high adsorption capacity, and mild synthesis conditions was chosen, and the optimal formulation of the shaped MIL-100(Fe) granules using different binders was explored. The high-performing MIL-100(Fe)@5PVB granule containing 5% polyvinyl butyral (PVB) with outstanding adsorption performance and mechanical strength was selected and massively prepared for AD system testing. It is found that, although binder content decreased the surface area, pore volume, and water uptake of MIL-100(Fe), the mechanical strength and adsorption kinetics of shaped MIL-100(Fe)@5PVB were enhanced, which favor its performance in an AD system. Moreover, system testing demonstrated that the desalination performance of the AD system based on the adsorption beds of MIL-100(Fe)@5PVB outperformed both silica gel and MIL-100(Fe) powder. The specific daily water production (SDWP) of the AD system based on MIL-100(Fe)@5PVB (28.74 m^3/ton/day) is 30% higher than that based on MIL-100(Fe) powder (19 m^3/ton/day). Such a phenomenon is mainly contributed by the improved water adsorption dynamics of MIL-100(Fe)@5PVB granules that favors the mass transfer efficiency in the adsorption bed. This work opens up the possibility for the development of high-performing shaped MOFs for adsorption desalination from the perspectives of formulation optimization and system testing.

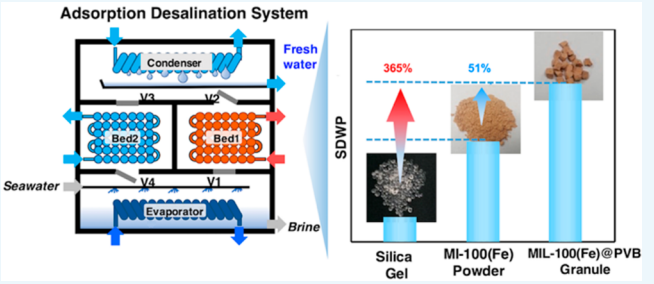

KEYWORDS: *water adsorption, shaped MIL-100(Fe), binders, specific daily water production, specific cooling power*

1. INTRODUCTION

With the demands of economic development and the improvement of living standards, global fresh water use has increased 6-fold in the last 100 years and is expected to continuously grow in the future.[1,2] Seawater desalination technology has been recognized as the solution to the fresh water crisis since the ocean covers 70% of the earth's surface. Currently, multistage flash (MSF), multieffect distillation (MED), and reverse osmosis (RO) technologies are widely used desalination techniques, which account for more than 90% of total capacity.[3] However, these desalination technologies may be accompanied by high energy consumption, excessive carbon emissions, and expensive equipment maintenance costs,[4,5] which cannot meet the demand of balanced development of environment and energy. Therefore, it is essential to develop a clean and renewable desalination technology with remarkably low energy consumption and carbon emissions.

Adsorption desalination (AD) driven by low-temperature heat sources (50−85 °C[5]) such as solar energy, geothermal energy, or industrial waste heat enables the wide use of renewable energy with reduced carbon emissions for water desalination and cooling. In the adsorption process, seawater evaporates in the evaporator and the resulting water vapor is continuously adsorbed by the adsorbents. In the desorption process, the desorbed water vapor enters the condenser to produce fresh water.[6,7] During the adsorption/desorption cycles, both desalinated water and cooling capacity can be produced. Thus, high-performing adsorbents are essential for desalination performance. Previous studies have focused on conventional adsorbents such as silica gels and zeolites. However, the unsatisfactory adsorption performance owing

Received: January 7, 2024
Revised: April 17, 2024
Accepted: April 18, 2024
Published: April 29, 2024

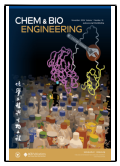

to the low adsorption capacity or high regeneration temperature limits their application in AD systems. The specific daily water production (SDWP) and specific cooling power (SCP) of the silica-gel-based AD system are usually unsatisfactory.[8]

In recent decades, metal−organic frameworks (MOFs) have been recognized as some of the most promising adsorbents owing to outstanding water adsorption capacities resulting from their ultrahigh surface areas and superior porosities.[9] Ou et al. even developed a sunlight-responsive MOF for water desalination which can produce 139.5 L of fresh water/kg of adsorbent/day.[10] Youssef et al.[11] reported that, at the regeneration temperature of 65 °C and evaporation temperature of 10 °C, Al fumarate displayed an SDWP of 3.4 m^3/ton/day and a specific cooling power (SCP) of 70.34 W/kg, which is 345 and 200% higher than those of AQSOA-Z02 and silica gel, respectively. AD system tests based on Al fumarate[6] also demonstrated its desalination performance superior to that of conventional silica gel at the chilled temperatures of 15 and 20 °C. It was also revealed that the maximum SDWP of 22.8 m^3/ton/day could be achieved by an AD system based on CPO-27(Ni) at an evaporator temperature of 40 °C, a condenser temperature of 5 °C, and a regeneration temperature of 95 °C.[12] Elsayed et al.[13,14] evaluated the desalination performance of three MOFs, i.e., CPO-27(Ni), Al fumarate, and MIL-101(Cr), by a Simulink model, in which MIL-101(Cr) exhibited the highest SDWP of 11 m^3/ton/day followed by Al fumarate (6.3 m^3/ton/day) and CPO-27(Ni) (4.6 m^3/ton/day). In order to improve the water adsorption performance of MOFs, chemical functionalization and ion doping become commonly used strategies. It has been reported that amino or hydroxyl functionalized and protonated MIL-53(Al) exhibited significantly increased water uptake and faster adsorption kinetics.[15] The improved SDWP has also been observed in functionalized aluminum fumarate, MOF-801(Zr), UiO-66(Zr),[16] protonated-amino-functionalized MIL-101(Cr), and MIL-125(Ti).[17]

However, experimentally synthesized MOFs were commonly used in powder form for AD systems. The direct use of powder MOFs may cause a series of problems such as equipment wear, pipe clogging, and pressure drop,[18−20] leading to low SDWP owing to the decreased water adsorption rate resulting from the high mass transfer resistance of powder. To avoid such issues, it is of great importance to develop shaped MOFs for enhanced desalination performance in AD systems.[21] However, the unbiased comparison of desalination performances of shaped MOFs and their counterparts in powder has yet to be explored. It has been reported that the framework of shaped MOFs obtained via pressurization may collapse with a dramatically reduced surface area, causing decreased adsorption capacity.[22] Thus, MOF shaping using binders is commonly used. However, physically mixing of binders with MOFs may impose negative effects on the adsorption capacity of MOF granules. The reduced hydrogen uptake of shaped Zr MOF using sucrose as binder has been reported.[23] Similarly, the slightly decreased acetylene uptake of four shaped MOFs, i.e., SIFSIX-3-Ni, SIFSIX-2-Cu-i, GEFSIX-2-Cu-i, and TIFSIX-2-Cu-i, using polyvinyl butyral (PVB) binder compared with their powder counterparts has also been reported, among which the shaped SIFSIX-2-Cu-i exhibited the highest adsorption capacity, indicating the dependence of adsorption capacity of shaped granules on the type of MOF.[24] Regardless of the decreased adsorption capacity, the improved mechanical strength of shaped MOFs has been frequently observed; for example, shaped MOF-801 using polyvinyl butyral (PVB) binder exhibits significantly higher mechanical stability than that using sucrose (SUC) binder.[25] In order to identify the best binder for aluminum fumarate, MIL-160(Al), and MIL-101(Cr), six hydrophilic organic binders were used to prepare 21 shaped MOFs, and it was found that 12 shaped MOFs exhibited negligible pore blocking effects, leading to water adsorption performances comparable with those of their powder counterparts. Besides, the increased hydrophilicity of shaped MIL-101(Cr) using hydrophilic binders favors the improved water uptake at low pressure.[26] Thus, choosing a proper binder is of great importance to ensure the high adsorption performance of shaped MOFs.

However, so far, only a few MOFs in powder form have been tested in AD systems mostly owing to their high cost and rigorous synthesis conditions. MIL-100(Fe) outperforms MIL-101(Cr)[9] owing to its facile synthesis at mild conditions for large-scale production.[27] It has also been reported that MIL-100(Fe) remains stable even after being exposed to boiling water for weeks or after 40 water adsorption (40 °C)/desorption (140 °C) cycles,[28] which enables it a suitable candidate for an AD system. In order to demonstrate the superior desalination performance of shaped MOFs, in this work, MIL-100(Fe) with high water stability, high adsorption capacity, and mild synthesis conditions was chosen, and the shaped MIL-100(Fe) granules were developed by formulation optimization based on four commonly used binders including polyvinyl butyral (PVB), hydroxyethyl cellulose (HEC), silica sol (SS), and sucrose (SUC) in varying contents. After the water adsorption performance and mechanical strength tests, the top candidate was selected and prepared in large scale, followed by a test in a manufactured two-bed AD system.

2. METHODOLOGY

2.1. Materials Synthesis. Ferrous chloride tetrahydrate ($FeCl_2 \cdot 4H_2O$, 98%) and polyvinyl butyral (PVB; $C_8H_{14}O_2 \cdot C_4H_6O_2 \cdot C_2H_4O$, MW = 90000−120000) were purchased from Shanghai Macklin Bio-Chem Technology Co. Benzene 1,3,5-tricarboxylic acid (H_3BTC, 98%), sucrose (SUC; $C_{12}H_{22}O_{11}$, AR), and hydroxyethyl cellulose (HEC; 3400−5000 mPa·s, 25 °C) were purchased from Shanghai Aladdin Bio-Chem Technology Co. Sodium hydroxide (NaOH, AR) and anhydrous ethanol (CH_3CH_2OH, AR) were purchased from Shanghai Sinopharm Chemical Reagent Co., Ltd. Neutral silica sol solution (SS; 30%) was purchased from Shanghai Yuanye Biotechnology Co., Ltd. Deionized water was prepared in the laboratory. All chemicals were used as received without any purification.

2.2. MIL-100(Fe) Powder and Shaped Granule Preparation. MIL-100(Fe) powder was synthesized under room temperature according to the literature[27] as described in section 1 of the Supporting Information. The shaped granules of MIL-100(Fe) were prepared using four binders (PVB, HEC, SUC, and SS). After dissolution of different amounts of binders in the solvent (HEC, SUC, SS in deionized water, PVB in ethanol), respectively, 5 wt % binder solution was added drop by drop to 0.9 g of MIL-100(Fe) powder at room temperature with constant stirring to obtain a viscous slurry. Then 1, 2, and 3 g of 5 wt % binder solution, respectively, were added to 0.9 g of MIL-100 (Fe) powder to prepare granules with different binder contents (5%/10%/15%). The above slurry was then dried at 80 °C in a mold, and the dried block was crushed and sieved to obtain granules with a granule size distribution of 2−3 mm.

The preparation details can be found in section 2 of the Supporting Information. Eventually, 12 MIL-100(Fe) granules with different binder contents (5%/10%/15%) were prepared for each binder. The prepared MIL-100(Fe) powder and shaped MIL-100(Fe)@5PVB samples are displayed in Figure 1.

https://doi.org/10.1021/cbe.4c00008
Chem Bio Eng. 2024, 1, 817−825

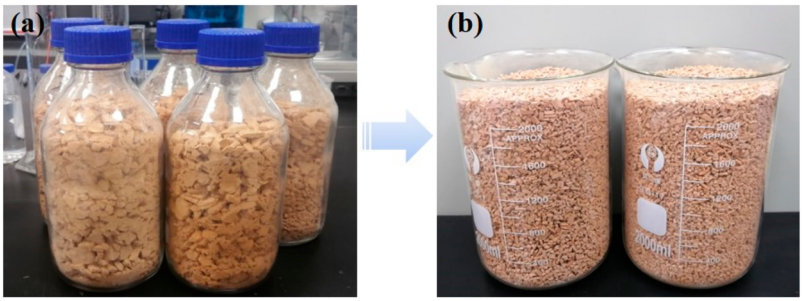

Figure 1. Prepared MIL-100(Fe) powder and (b) MIL-100(Fe)@5PVB granules.

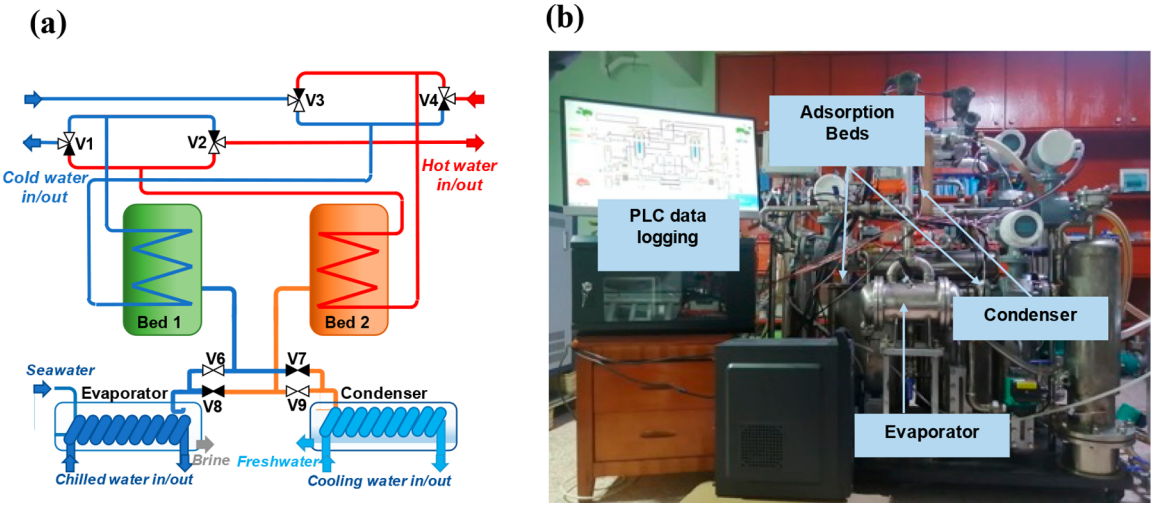

Figure 2. Schematic diagram (a) and photograph (b) of the adsorption desalination system.

2.3. Characterization and Tests. The samples were characterized by powder X-ray diffraction (PXRD) and scanning electron microscopy (SEM), respectively (see details in section 3 of the Supporting Information). The structure properties including surface area, pore volume, and pore size distribution (PSD) were obtained from N_2 adsorption isotherms at 77 K. Thermogravimetric analysis was carried out on a Diamond thermogravimetric/differential thermal analysis (TG/DTA) instrument using a heating rate of 20 °C/min under flowing nitrogen. The mechanical strength of samples was tested using a CMT4104 electronic universal testing machine. Water adsorption isotherms of the samples were measured with a gas adsorption analyzer by an Autosorb-iQ2 from Quantachrome Instruments at 298 K. Water adsorption rates of samples were tested in a constant temperature and humidity chamber.

2.4. AD System Test of Shaped MIL-100(Fe). The AD system was designed and manufactured for the desalination performance test, which mainly consists of two identical adsorption beds, an evaporator, and a condenser (Figure 2). A complete operation cycle of AD includes four steps: (1) The first step is the switching process in which hot water is introduced into bed 1 and cold water into bed 2 by controlling electric valves. When bed 1 is preheated, bed 2 is precooled. At this stage, the valves between the beds and the evaporator/condenser are closed. (2) The second step is the adsorption/desorption process in which the valve between bed 2 and the evaporator is opened to allow adsorption and evaporation, while the valve between bed 1 and the condenser is opened to allow the desorption of water vapor from bed 1. In this process, the evaporator and condenser output cooling and fresh water, respectively. This process goes through one half cycle, followed by another half cycle. (3) The third step is the switching process in which the valves between the beds and the evaporator and condenser are closed again. When bed 1 is precooled, bed 2 is preheated. (4) In the end of the adsorption/desorption process, the modes of the two beds are switched.

In order to simulate the operating conditions, a hot water tank with a volume of 12 L was used to provide heat for desorption. At the same time, a chilled water tank equipped with a 1 kW heater was used to provide chilled water. Seawater supply and freshwater collection devices were also installed. A programmable logic controller (PLC) was used to control the electric valves and pumps. Four electromagnetic flow meters and eight platinum resistance temperature sensors were used to measure the flows and temperatures of hot water, cold water, chilled water, and cooling water in real time. Four pressure transmitters for measuring the pressure profile of the system were also employed. Simulated seawater was prepared using 3.5 wt % NaCl solution. MIL-100(Fe)@5PVB granules (Figure 1b) were packed between the fins of the exchanger (Figure 3) and covered with wire mesh. The structure parameters of the adsorption bed are provided in Table 1.

Two parameters including specific daily water production (SDWP) and specific cooling power (SCP) were used for assessing the adsorption desalination performance. SDWP is the amount of fresh water produced per tonne of adsorbent per day. SCP is the amount of cooling produced per unit mass of adsorbent. These parameters can be obtained using the following equations.

$$Q_{con} = \frac{\sum_{i=1}^{n} C_p m_{cooling}(T_{i,cooling,out} - T_{i,cooling,in})}{n} \quad (1)$$

$$SDWP = \frac{86400 Q_{con}}{M_a r_w} \quad (2)$$

$$Q_{eva} = \frac{\sum_{i=1}^{n} C_p m_{chilled}(T_{i,chilled,in} - T_{i,chilled,out})}{n} \quad (3)$$

https://doi.org/10.1021/cbe.4c00008
Chem Bio Eng. 2024, 1, 817−825

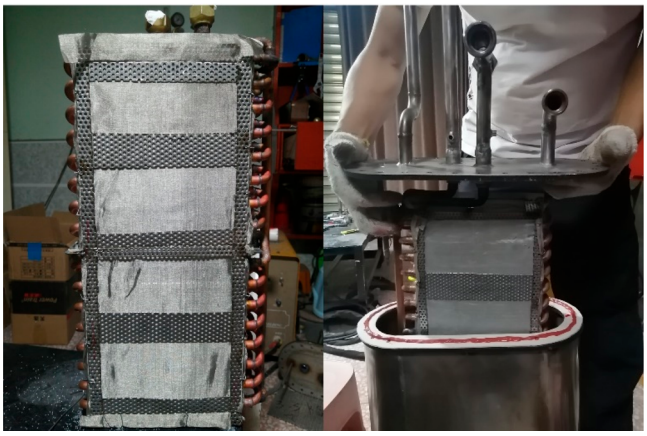

Figure 3. Photograph of adsorption bed.

Table 1. Parameters of Wire Finned Tubes Heat Exchanger in Adsorption Bed

parameter	value	units
length	415	mm
width	175	mm
fin pitch	3	mm
fin thickness	0.12	mm
tube outer diameter	9.52	mm
tube thickness	0.3	mm
number of heat exchangers/bed	2	
adsorbent/bed	0.435	kg
adsorption bed metal mass	1.6	kg

$$\mathrm{SCP} = \frac{Q_{\mathrm{eva}}}{M_{\mathrm{a}}} \tag{4}$$

M_a is the mass of adsorbent in the adsorption bed (kg), r_w is the latent heat of condensation of fresh water (kJ/kg), and $m_{cooling}$ and $m_{chilled}$ are the mass flow rates of cooling water and chilled water, respectively. $T_{i,cooling,out}$ and $T_{i,cooling,in}$ are the temperatures of cooling water outflow and inflow to the condenser, respectively. $T_{i,chilled,in}$ and $T_{i,chilled,out}$ are the temperatures of chilled water inflow and outflow to the evaporator, respectively, and n is the number of data collected during the test.

3. RESULTS AND DISCUSSION

3.1. Structure Characterization of Shaped MIL-100(Fe). The structure properties of MOFs are usually modified upon shaping with binders. Thus, structure characterization of the shaped MIL-100(Fe) granules by powder X-ray diffraction (PXRD) was carried out. It is found that the crystal structure of MIL-100(Fe) was not remarkably disrupted during the shaping process according to PXRD patterns of shaped MIL-100(Fe)@SUC (Figure 4a), MIL-100(Fe)@SS (Figure 4b), MIL-100(Fe)@HEC (Figure 4c), and MIL-100(Fe)@PVB (Figure 4d) regardless of the different binder types and contents. The typical peaks in PXRD patterns of MIL-100(Fe) are not changed upon binder integration. This is because shaped MIL-100(Fe) granules were prepared by mixing the as-prepared MIL-100(Fe) powder with binder molecules. Both the smaller SUC molecules that possibly enter the pores of MIL-100(Fe) and the big-sized HEC, SS, and PVB molecules that are mostly present on the outer surface of MOF crystal particles cannot disrupt the crystal structure of MIL-100(Fe). At the high binder content, the peak intensity at $2\theta \approx 4.15°$ and $2\theta \approx 6.45°$ of shaped MIL-100(Fe) granules with high binder content (i.e., MIL-100(Fe)@15HEC, MIL-100(Fe)@15PVB) is slightly lower than that of the powder. Such a trend can be ascribed to the dilution effects of MIL-100(Fe) after mixing with binders, which has been demonstrated in previous reports on shaped MIL-160(Al) and MIL-101(Cr).[29,30]

The textural properties of the granules including BET surface area, pore volume (Table 2), and pore size distribution (PSD) that directly correlate with water adsorption performance were obtained based on the N_2 adsorption isotherms at 77 K (Figure S3). It was found that both the BET surface area and pore volume of the shaped granules were lower than those of the powder (S_{BET} = 1983.2 m^2/g, V_{total} = 1.196 cm^3/g), and the higher the binder content, the lower the surface area and pore volume. This may be due to the pore blockage effects of binders in shaped samples. The pore size distributions of MIL-100(Fe)@SUC (Figure 5a), MIL-100(Fe)@SS (Figure 5b), MIL-100(Fe)@HEC (Figure 5c), and MIL-100(Fe)@PVB (Figure 5d) substantiated this anticipation, in which the volume fraction of each pore in shaped granules is deceased with increasing binder content, but no remarkable pore size variation was inspected. Owing to the smaller molecular size

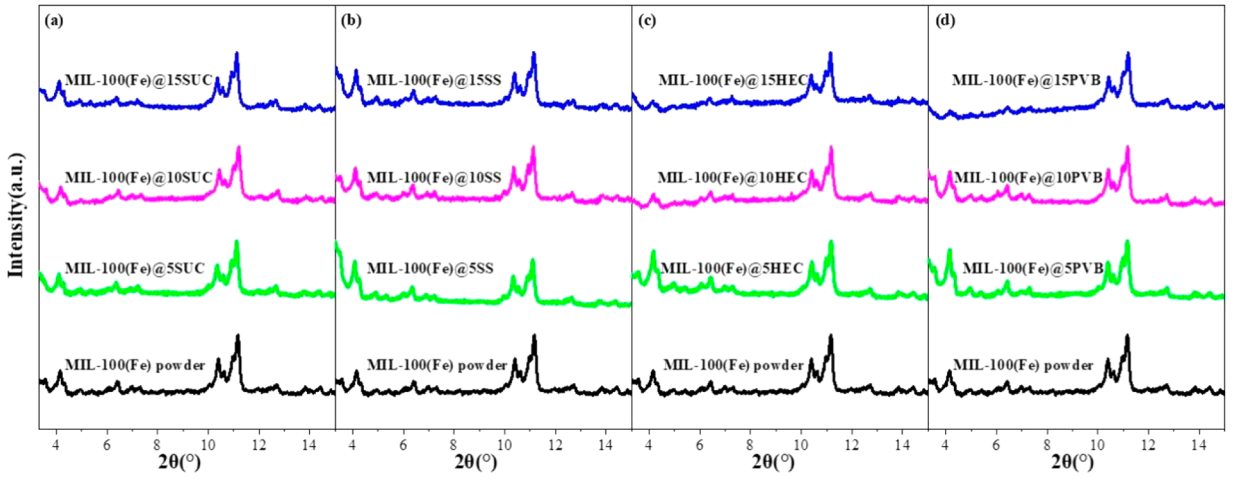

Figure 4. PXRD patterns of MIL-100(Fe) granules and powder: (a) MIL-100(Fe)@SUC, (b) MIL-100(Fe)@SS, (c) MIL-100(Fe)@HEC, and (d) MIL-100(Fe)@PVB.

https://doi.org/10.1021/cbe.4c00008
Chem Bio Eng. 2024, 1, 817−825

Table 2. Textural Properties of MIL-100(Fe) Granules and Powder

sample	S_{BET} (m^2/g)	pore volume (cm^3/g)	
		V_{total} [a]	V_{micro} [b]
MIL-100(Fe) powder	1983.2	1.196	0.638
MIL-100(Fe)@5PVB	1713.1	1.022	0.540
MIL-100(Fe)@10PVB	1534.2	0.916	0.482
MIL-100(Fe)@15PVB	1431.6	0.823	0.459
MIL-100(Fe)@5SS	1616.6	1.063	0.508
MIL-100(Fe)@10SS	1550.2	1.004	0.506
MIL-100(Fe)@15SS	1409.3	0.860	0.432
MIL-100(Fe)@5HEC	1536.0	0.877	0.495
MIL-100(Fe)@10HEC	1517.5	0.856	0.484
MIL-100(Fe)@15HEC	1389.1	0.805	0.442
MIL-100(Fe)@5SUC	1547.1	0.933	0.499
MIL-100(Fe)@10SUC	1438.4	0.857	0.463
MIL-100(Fe)@15SUC	1245.0	0.748	0.383

[a]Measured at P/P_0 = 0.995. [b]Calculated by *t*-plot.

and hydrophilicity of SUC, there is a high possibility for SUC to enter the pores of MIL-100(Fe), thus leading to the significantly decreased surface area and pore volume of shaped MIL-100(Fe)@SUC. Differently, for the large molecular sized polymer binders including PVB and HEC as well as the larger colloidal particle size of SS, it is difficult for them to enter the pores of MIL-100(Fe). Thus, there is a higher chance for these binders to encapsulate the MIL-100(Fe) crystal surface, leading to the blockage of some pore apertures on the crystal surface. Thus, similarly decreased surface area and pore volume can be observed. Compared with hydrophilic HEC and SS, the butyraldehyde and acetate groups of PVB enable its high hydrophobicity,[24,31] which causes less evident pore blockage. Therefore, the surface area and pore volume of shaped MIL-100(Fe) using PVB binders are mostly retained (Figure 5d).

3.2. Water Adsorption Performance of Shaped MIL-100(Fe). Similar to the structure properties, the equilibrium water adsorption isotherms of the shaped MIL-100(Fe)@SUC (Figure 6a), MIL-100(Fe)@SS(Figure 6b), MIL-100(Fe)@HEC (Figure 6c), and MIL-100(Fe)@PVB (Figure 6d) exhibited decreased water uptake compared to powder sample regardless of binder type and content. However, the shape of the adsorption isotherm of MIL-100(Fe) powder with two steps at P/P_0 = 0.25 and P/P_0 = 0.4 was not changed upon shaping, indicating similar adsorption behaviors of water molecules in shaped samples. At low pressure, water adsorption mostly occurs around metal sites of the large pores, where water clusters around the hydrophilic sites may formed. The two steps may correspond to continuous filling of two types of pores in MIL-100(Fe).[21,32] The step position of the isotherms of some MIL-100(Fe) granules slightly shifted toward high pressure, which may be ascribed to the evidently decreased micropores below 2 nm as evidenced by the PSD of Figure 5 that enhances the hydrophobicity of adsorbents.

Moreover, the water adsorption capacities of all shaped samples decreased with the increase of binder content, among which MIL-100(Fe)@5PVB exhibited the highest water capacity with a water adsorption capacity of 0.485 g/g at P/P_0 = 0.9. With the increase of binder content, the adsorption capacity of the shaped MIL-100(Fe) granules using SUC binders showed a significant decrease. Such a trend is mostly due to the evidently decreased surface area and pore volume of MIL-100(Fe)@SUC granules (Table 2), since the smallest size and high hydrophilicity enable the entrance of more SUC binder molecules. In contrast, SS, HEC, and PVB binder molecules are much bigger and are difficult to penetrate into the pores of MIL-100(Fe). Instead, these binder molecules tend to cover the outer surface of the MOF crystal, leading to aperture blockage to some extent. Nevertheless, SS and HEC are hydrophilic but PVB is strongly hydrophobic. Thus, although the surface area and pore volumes of MIL-100(Fe)@SS, MIL-100(Fe)@HEC, and MIL-100(Fe)@PVB are also decreased, the water uptakes of high-binder-content MIL-100(Fe)@SS and MIL-100(Fe)@HEC are higher than that of MIL-100(Fe)@PVB owing to the strong hydrophobicity of PVB binders. Their equilibrium water uptakes of high-binder-content MIL-100(Fe) granules at P/P_0 = 0.9 still outperform the silica gel (~0.35 g/g) and zeolite (0.1−0.3 g/g).[33]

3.3. Mechanical Strength and Water Adsorption Dynamics of MIL-100(Fe)@PVB. Except for the water adsorption performance, the mechanical strength of shaped samples was also tested with an electronic universal testing machine (Figure 7a). Based on the stress−strain curves (Figure 7b), it is revealed that, although the strength of the shaped

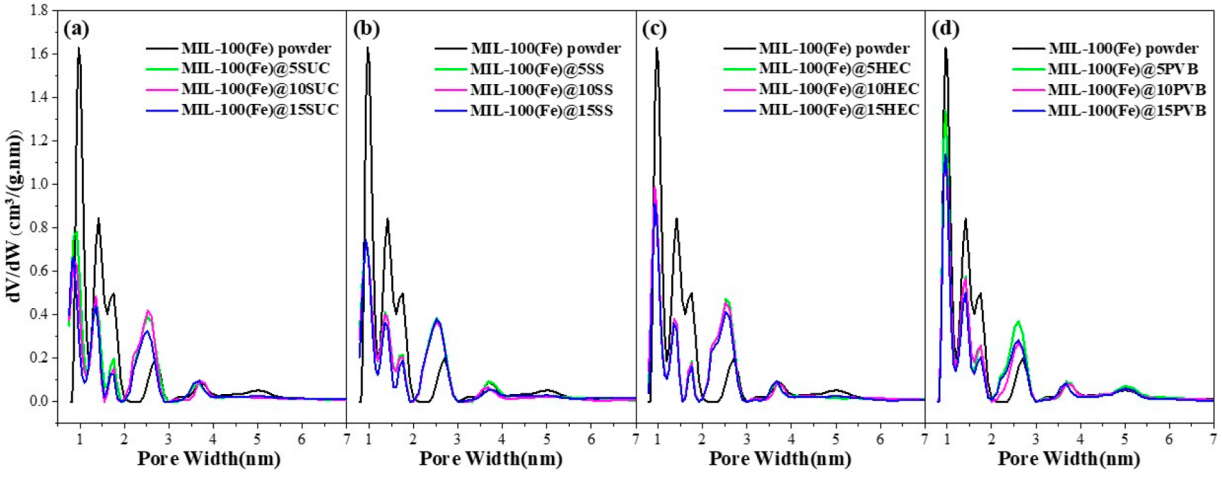

Figure 5. Pore size distributions of MIL-100(Fe) granules and powder: (a) MIL-100(Fe)@SUC, (b) MIL-100(Fe)@SS, (c) MIL-100(Fe)@HEC, and (d) MIL-100(Fe)@PVB.

https://doi.org/10.1021/cbe.4c00008
Chem Bio Eng. 2024, 1, 817−825

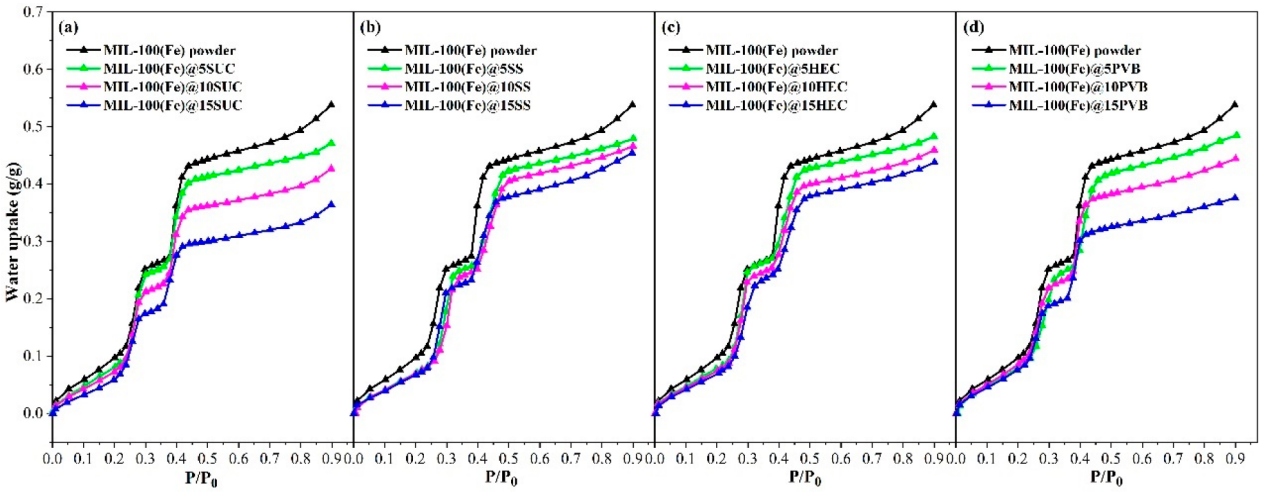

Figure 6. Effect of binders and percentage on the water adsorption capacity of MIL-100(Fe) granules at 298 K: (a) MIL-100(Fe)@SUC, (b) MIL-100(Fe)@SS, (c) MIL-100(Fe)@HEC, and (d) MIL-100(Fe)@PVB.

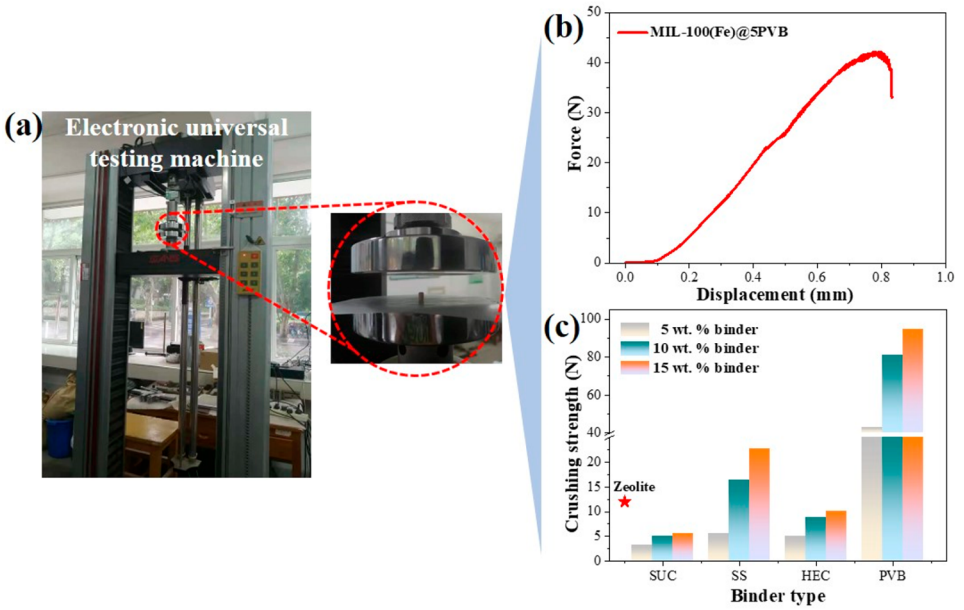

Figure 7. (a) Single granule mechanical strength test instrument, (b) stress−strain curves, and (c) strength results for all granules.

MIL-100(Fe) granules increases with binder content, the shaped samples using PVB binder exhibit significantly higher crushing strength than other samples using SS, HEC, and SUC binders (Figure 7c). This is probably due to the presence of a large number of hydroxyl, butyral, and acetic acid groups in PVB molecules, which possess high affinity toward both organic and inorganic materials, leading to mechanical strength improvement of shaped MIL-100(Fe). Although the strength of the shaped granules prepared using SS and HEC binders is not outstanding, they outperform commercial zeolite 4A granules (~13 N).[34] The thermogravimetric analysis (Figure S4) suggested that the thermal stability of MIL-100(Fe)@5PVB granules is nearly unchanged compared with MIL-100(Fe) powder. Considering both the retained water adsorption capacity and crushing strength of shaped samples, MIL-100(Fe)@5PVB with a crushing strength of approximately 42 N was selected for a further AD system test.

Before the system test, to ensure the superiority of shaped samples, the adsorption kinetics of MIL-100(Fe)@5PVB and MIL-100(Fe) powder were evaluated (Figure 8). It is disclosed that, although the equilibrium water adsorption capacity of MIL-100(Fe) powder is higher than that of MIL-100(Fe)@5PVB, the adsorption rate of MIL-100(Fe)@5PVB is faster. Compared with the MIL-100(Fe) powder consisting of micrometer sized crystal particles, the shaped MIL-100(Fe)@5PVB composed of millimeter sized granules favors enhanced permeability and decreased flow resistance, leading to an increased adsorption rate.[35] On the other hand, the increased mesopore percentage of MIL-100(Fe)@5PVB is also beneficial to the molecular diffusion and Knudsen diffusion of water vapor within the granules.[35] Such a result suggests the higher porosity and lower pressure drop in the adsorption bed of MIL-100(Fe)@5PVB granules than MIL-100(Fe) powder, which is favorable for desalination performance in the AD system.

https://doi.org/10.1021/cbe.4c00008
Chem Bio Eng. 2024, 1, 817−825

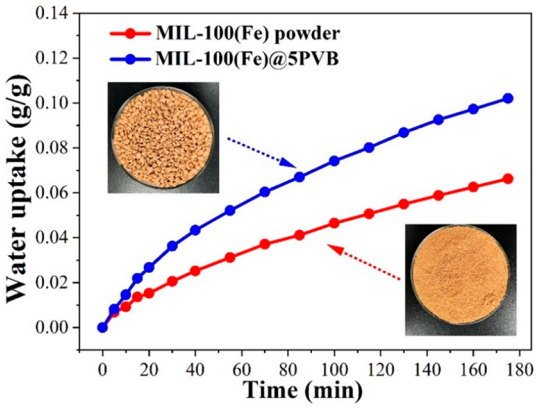

Figure 8. Dynamic adsorption curves of MIL-100(Fe) powder and MIL-100(Fe)@5PVB (T = 298 K and RH = 60%).

3.4. AD Performance of MIL-100(Fe)@5PVB. Based on the above results, 870 g of MIL-100(Fe)@5PVB was prepared for a system test. The temperatures of hot water (T_{hot}) for desorption, cold water (T_{cold}) for precooling the adsorption bed, cooling water ($T_{cooling}$) passing through the condenser, and chilled water ($T_{chilled}$) passing through the evaporator impose effects on the performance of the AD system. In this work, a typical operation condition of T_{hot} = 80 °C, T_{cold} = 25 °C, $T_{chilled}$ = 20 °C, and $T_{cooling}$ = 20 °C was employed according to the literature.[36] During the adsorption/desorption cycle of the system, since the times for adsorption and desorption are identical, the half time cycle ($t_{half\ cycle}$) is defined as the time for the adsorption or desorption process. In order to identify the optimum time for the adsorption/desorption cycle, the performance of the AD system based on MIL-100(Fe)@5PVB was tested first at different half time cycles of $t_{half\ cycle}$ = 400, 600, 800, and 1000 s. It was found that both the freshwater production (SDWP) and cooling capacity (SCP) of the system (Figure 9) increased until $t_{half\ cycle}$ = 600 s and then decreased with the increase of the $t_{half\ cycle}$. Such a result demonstrates that either a too short or a too long $t_{half\ cycle}$ is unfavorable for the SDWP and SCP of the AD system. If $t_{half\ cycle}$ is too short, there is not sufficient time for the adsorbents to achieve equilibrium or saturation uptake, resulting in poor water uptake and an unsatisfactory desalination performance. Besides, for a short $t_{half\ cycle}$, the adsorption bed will be heated and cooled frequently within a short time period, leading to serious energy consumption that is detrimental to the energy utilization efficiency of the system. However, when $t_{half\ cycle}$ is too long, it takes a much longer time for heating and cooling of adsorption beds, which in turn significantly slows down the adsorption/desorption rate, leading to low water production and cooling capacity. According to Figure 9, the optimal $t_{half\ cycle}$ for the AD system based on MIL-100(Fe)@5PVB is 600 s.

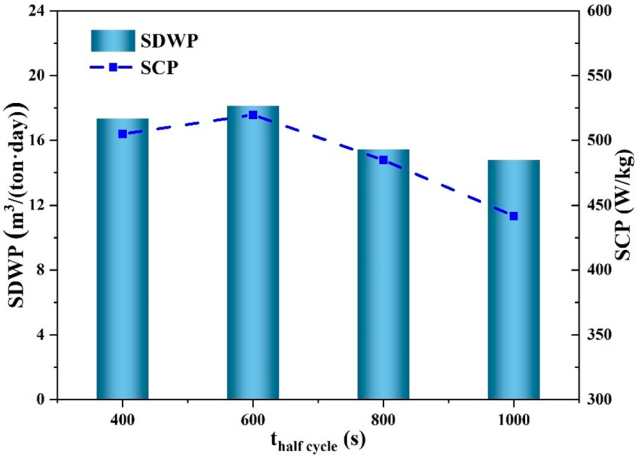

Figure 9. Desalination and cooling performance of MIL-100(Fe)@5PVB at different $t_{half\ cycle}$ values (T_{hot} = 80 °C, T_{cold} = 25 °C, $t_{switching}$ = 70 s, $T_{cooling}$ = 20 °C, $T_{chilled}$ = 20 °C).

In order to verify the excellent desalination performance of MIL-100(Fe)@5PVB granules, the adsorption desalination performance of the conventional adsorbent silica gel was also tested at an identical operation condition (T_{hot} = 80 °C, T_{cold} = 25 °C, $T_{chilled}$ = 20 °C, $T_{cooling}$ = 20 °C). It was revealed that the optimal $t_{half\ cycle}$ of the AD system based on silica gel is 800 s (Figure S5); thus the SDWP and SCP at $t_{half\ cycle}$ = 800 s were used. In addition, the SDWP of an AD system based on MIL-100(Fe) in powder form obtained from identical working conditions in the literature[9] was also adopted for comparison. It was demonstrated that the SDWP and SCP of MIL-100(Fe)@5PVB were about 3 times higher than those of silica gel regardless of the chilled water temperature (Figure 10).

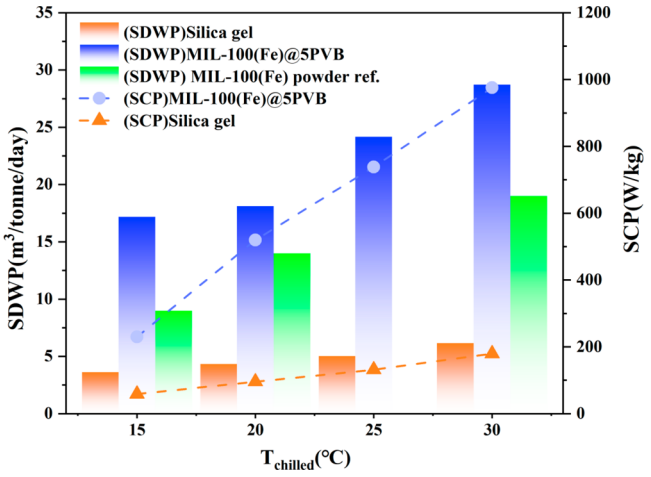

Figure 10. Adsorption desalination comparative study between silica gel, MIL-100(Fe), and MIL-100(Fe)@5PVB. The operation conditions for MIL-100(Fe)@5PVB and silica gel are identical: T_{cold} = 25 °C, $T_{cooling}$ = 20 °C, and T_{hot} = 80 °C. MIL-100(Fe) powder was tested at $t_{half\ cycle}$ = 700 s, T_{cold} = 30 °C, $T_{cooling}$ = 20 °C, and T_{hot} = 95 °C.

Compared with MIL-100(Fe) powder, the SDWP of MIL-100(Fe)@5PVB granules is significantly higher, which is improved by approximately 300% at $T_{chilled}$ = 15 °C and 50% at $T_{chilled}$ = 30 °C. Such a trend can be ascribed to the improved water adsorption rate of MIL-100(Fe)@5PVB resulting from its decreased mass transfer resistance compared with MIL-100(Fe) powder, resulting in an outstanding freshwater production performance. Such results illustrate the counterbalance between the water adsorption capacity and adsorption kinetics of shaped MOFs, which may dominate their performance in systems.

https://doi.org/10.1021/cbe.4c00008
Chem Bio Eng. 2024, 1, 817−825

4. CONCLUSION

In order to demonstrate the superiority of shaped MOFs for adsorption desalination, in this work, MIL-100(Fe) with high water stability and adsorption performance was chosen for shaped MOF development. In order to identify the optimum formulation for shaped MIL-100(Fe), 12 shaped granules using four different binders (i.e., SUC, HEC, PVB, and SS) and contents (5, 10, and 15%) were prepared, characterized, and tested for adsorption desalination. It is revealed that, although the crystallinity of MIL-100(Fe) was not disrupted by shaping using binders, the structure properties including the surface area and pore volume of shaped MIL-100(Fe) were decreased owing to the pore blockage by binder molecules. Among the shaped granules, MIL-100(Fe)@5PVB granules with 5% PVB content exhibiting both excellent water adsorption performance and mechanical strength were selected for large-scale production and system tests. AD system tests revealed that, at the optimal $t_{half\,cycle}$ of 600 s, the system based on MIL-100(Fe)@5PVB exhibited 3 times higher SDWP (28.74 m^3/ton/day) than silica gel (6.17 m^3/ton/day), which is almost 30% higher than that of MIL-100(Fe) in powder form (19 m^3/ton/day). Such a trend is mainly attributed to the outstanding water adsorption rate of MIL-100(Fe)@5PVB that favors the mass transfer efficiency in an AD system. This study paves the way for the development of shaped MOFs for AD system application from the perspective of materials science and thermal engineering. It should be noted that both binder type and MOF type may impose significant impacts on the adsorption performance of shaped granules. Therefore, the formulation optimization is necessary for each type of MOF. Besides, given the high costs and low yields of most MOFs, not all shaped MOFs can be tested in the AD system, which is the main limitation for the exploration of high-performing MOFs for adsorption desalination.

■ ASSOCIATED CONTENT

Supporting Information

The Supporting Information is available free of charge at https://pubs.acs.org/doi/10.1021/cbe.4c00008.

Additional MIL-100(Fe) powder and granule preparation details, structure and morphology characterization and mechanical strength test details, SEM images, nitrogen adsorption isotherms, thermogravimetric analysis and effect of half cycle time on the performance of silica gel desalination system (PDF)

■ AUTHOR INFORMATION

Corresponding Author

Song Li − *Department of New Energy Science and Engineering, School of Energy and Power Engineering and China−EU Institute for Clean and Renewable Energy, Huazhong University of Science and Technology, Wuhan 430074, China;* orcid.org/0000-0003-3552-3250; Email: songli@hust.edu.cn

Authors

Hao Chen − *Department of New Energy Science and Engineering, School of Energy and Power Engineering, Huazhong University of Science and Technology, Wuhan 430074, China*

Qiancan Wang − *Department of New Energy Science and Engineering, School of Energy and Power Engineering and China−EU Institute for Clean and Renewable Energy, Huazhong University of Science and Technology, Wuhan 430074, China*

Long Chen − *Department of New Energy Science and Engineering, School of Energy and Power Engineering and China−EU Institute for Clean and Renewable Energy, Huazhong University of Science and Technology, Wuhan 430074, China*

Shanshan Cai − *Department of New Energy Science and Engineering, School of Energy and Power Engineering and China−EU Institute for Clean and Renewable Energy, Huazhong University of Science and Technology, Wuhan 430074, China*

Jing Lei − *Shenzhen Angel Drinking Water Industrial Group Corporation, Shenzhen 518108, China*

Complete contact information is available at: https://pubs.acs.org/10.1021/cbe.4c00008

Notes

The authors declare no competing financial interest.

■ ACKNOWLEDGMENTS

This work was supported by the National Key Research and Development Program (No. 2020YFB1506300). We thank the Huazhong University of Science and Technology Analytical & Testing Center for providing support on material characterization.

■ ABBREVIATIONS

AD	adsorption desalination
SDWP	specific daily water production, m^3/ton/day
SCP	specific cooling power, W/kg
MOF	metal−organic framework
MED	multieffect distillation
MSF	multistage flash evaporation
RO	reverse osmosis
PVB	polyvinyl butyral
HEC	hydroxyethyl cellulose
SS	silica sol
SUC	sucrose

Variables

P	pressure, Pa
Q	heat, W
M_a	mass of adsorbent, kg
C^p	specific heat capacity, J/(kg·K)
r_w	water latent heat, J/kg
P_0	saturated pressure, Pa
q	water uptake, kg/kg
Δq	working adsorption capacity, kg/kg
T	temperature, K
t	time, s
m	mass flow rate, kg/s

Subscripts

ads	adsorption
des	desorption
cold	cold water
hot	hot water
chilled	chilled water
cooling	cooling water
half cycle	half cycle time
switching	switching time
con	condensation

eva evaporation

REFERENCES

(1) Ghaffour, N.; Soukane, S.; Lee, J. G.; Kim, Y.; Alpatova, A. Membrane Distillation Hybrids for Water Production and Energy Efficiency Enhancement: A Critical Review. *Appl. Energy* **2019**, *254*, 113698.

(2) U.N. *The United Nations World Water Development Report 2021*; The United Nations: 2021.

(3) Alnajdi, O.; Wu, Y.; Kaiser Calautit, J. Toward a Sustainable Decentralized Water Supply: Review of Adsorption Desorption Desalination (ADD) and Current Technologies: Saudi Arabia (SA) as a Case Study. *Water* **2020**, *12*, 1111.

(4) Mezher, T.; Fath, H.; Abbas, Z.; Khaled, A. Techno-economic Assessment and Environmental Impacts of Desalination Technologies. *Desalination* **2011**, *266*, 263−273.

(5) Hua, W. S.; Xu, H. J.; Xie, W. H. Review on Adsorption Materials and System Configurations of the Adsorption Desalination Applications. *Appl. Therm. Eng.* **2022**, *204*, 117958.

(6) Elsayed, E.; AL-Dadah, R.; Mahmoud, S.; Anderson, P.; Elsayed, A. Experimental Testing of Aluminium Fumarate MOF for Adsorption Desalination. *Desalination* **2020**, *475*, 114170.

(7) Saleh, M. M.; Elsayed, E.; AL-Dadah, R.; Mahmoud, S. Experimental Testing of Wire Finned Heat Exchanger Coated with Aluminium Fumarate MOF Material for Adsorption Desalination Application. *Therm. Sci. Eng. Prog.* **2022**, *28*, 101050.

(8) Wang, X.; Ng, K. C. Experimental Investigation of an Adsorption Desalination Plant Using Low-temperature Waste Heat. *Appl. Therm. Eng.* **2005**, *25*, 2780−2789.

(9) AL-Dadah, R.; Mahmoud, S.; Elsayed, E.; Youssef, P.; Al-Mousawi, F. Metal-organic Framework Materials for Adsorption Heat Pumps. *Energy* **2020**, *190*, 116356.

(10) Ou, R.; Zhang, H.; Truong, V. X.; Zhang, L.; Hegab, H. M.; Han, L.; Hou, J.; Zhang, X.; Deletic, A.; Jiang, L.; et al. A Sunlight-responsive Metal−organic Framework System for Sustainable Water Desalination. *Nat. Sustain.* **2020**, *3*, 1052−1058.

(11) Youssef, P.; Mahmoud, S.; Al-Dadah, R.; Elsayed, E.; El-Samni, O. Numerical Investigation of Aluminum Fumarate MOF Adsorbent Material for Adsorption Desalination/Cooling Application. *Energy Procedia* **2017**, *142*, 1693−1698.

(12) Youssef, P. G.; Dakkama, H.; Mahmoud, S. M.; AL-Dadah, R. K. Experimental Investigation of Adsorption Water Desalination/Cooling System Using CPO-27Ni MOF. *Desalination* **2017**, *404*, 192−199.

(13) Elsayed, E.; AL-Dadah, R.; Mahmoud, S.; Anderson, P. A.; Elsayed, A.; Youssef, P. G. CPO-27(Ni), Aluminium Fumarate and MIL-101(Cr) MOF Materials for Adsorption Water Desalination. *Desalination* **2017**, *406*, 25−36.

(14) Elsayed, E.; AL-Dadah, R.; Mahmoud, S.; Elsayed, A.; Anderson, P. A. Aluminium Fumarate and CPO-27(Ni) MOFs: Characterization and Thermodynamic Analysis for Adsorption Heat Pump Applications. *Appl. Therm. Eng.* **2016**, *99*, 802−812.

(15) Han, B.; Chakraborty, A. Functionalization, Protonation and Ligand Extension on MIL-53 (Al) MOFs to Boost Water Adsorption and Thermal Energy Storage for Heat Transformations. *Chem. Eng. J.* **2023**, *472*, 145137.

(16) Han, B.; Chakraborty, A. Evaluation on the Performances of Adsorption Desalination Employing Functionalized Metal-organic Frameworks (MOFs). *Appl. Therm. Eng.* **2023**, *218*, 119365.

(17) Han, B.; Chakraborty, A. Highly Efficient Adsorption Desalination Employing Protonated-amino-functionalized MOFs. *Desalination* **2022**, *541*, 116045.

(18) Liu, X.; Xie, L.; Wu, Y. Recent Advances in the Shaping of Metal-organic Frameworks. *Inorg. Chem. Front.* **2020**, *7*, 2840−2866.

(19) Ryu, U.; Jee, S.; Rao, P. C.; Shin, J.; Ko, C.; Yoon, M.; Park, K. S.; Choi, K. M. Recent Advances in Process Engineering and Upcoming Applications of Metal−organic Frameworks. *Coord. Chem. Rev.* **2021**, *426*, 213544.

(20) Akhtar, F.; Andersson, L.; Ogunwumi, S.; Hedin, N.; Bergstrom, L. Structuring Adsorbents and Catalysts by Processing of Porous Powders. *J. Eur. Ceram. Soc.* **2014**, *34*, 1643−1666.

(21) Iacomi, P.; Lee, U.; Valekar, A. H.; Chang, J.; Llewellyn, P. L. Investigating the Effect of Alumina Shaping on the Sorption Properties of Promising Metal−organic Frameworks. *Rsc Adv.* **2019**, *9*, 7128−7135.

(22) Wang, Z.; Liu, L.; Li, Z.; Goyal, N.; Du, T.; He, J.; Li, G. K. Shaping of Metal−Organic Frameworks: A Review. *Energy Fuels* **2022**, *36*, 2927−2944.

(23) Ren, J.; Musyoka, N. M.; Langmi, H. W.; Swartbooi, A.; North, B. C.; Mathe, M. A More Efficient Way to Shape Metal-organic Framework (MOF) Powder Materials for Hydrogen Storage Applications. *Int. J. Hydrog. Energy* **2015**, *40*, 4617−4622.

(24) Zheng, J.; Cui, X.; Yang, Q.; Ren, Q.; Yang, Y.; Xing, H. Shaping of Ultrahigh-loading MOF Pellet with a Strongly Anti-tearing Binder for Gas Separation and Storage. *Chem. Eng. J.* **2018**, *354*, 1075−1082.

(25) Taddei, M.; McPherson, M. J.; Gougsa, A.; Lam, J.; Sewell, J.; Andreoli, E. An Optimised Compaction Process for Zr-Fumarate (MOF-801). *Inorganics* **2019**, *7*, 110.

(26) Hastürk, E.; Höfert, S.; Topalli, B.; Schlüsener, C.; Janiak, C. Shaping of MOFs via Freeze-casting Method With Hydrophilic Polymers and Their Effect on Textural Properties. *Microporous Mesoporous Mater.* **2020**, *295*, 109907.

(27) Guesh, K.; Caiuby, C. A. D.; Mayoral, Á.; Díaz-García, M.; Díaz, I.; Sanchez-Sanchez, M. Sustainable Preparation of MIL-100(Fe) and Its Photocatalytic Behavior in the Degradation of Methyl Orange in Water. *Cryst. Growth Des.* **2017**, *17*, 1806−1813.

(28) Jeremias, F.; Khutia, A.; Henninger, S. K.; Janiak, C. MIL-100(Al, Fe) as Water Adsorbents for Heat Transformation Purposes—a Promising Application. *J. Mater. Chem.* **2012**, *22*, 10148−10151.

(29) Gökpinar, S.; Ernst, S.; Hastürk, E.; Möllers, M.; El Aita, I.; Wiedey, R.; Tannert, N.; Nießing, S.; Abdpour, S.; Schmitz, A.; et al. Air-Con Metal−Organic Frameworks in Binder Composites for Water Adsorption Heat Transformation Systems. *Ind. Eng. Chem. Res.* **2019**, *58*, 21493−21503.

(30) Valekar, A. H.; Cho, K.; Lee, U.; Lee, J. S.; Yoon, J. W.; Hwang, Y. K.; Lee, S. G.; Cho, S. J.; Chang, J. Shaping of Porous Metal−organic Framework Granules Using Mesoporous ρ-alumina as a Binder. *Rsc Adv.* **2017**, *7*, 55767−55777.

(31) Valekar, A. H.; Lee, S.; Kim, Y. K.; Cho, K. H.; Jo, D.; Hwang, Y. K.; Yoon, J. W.; Lee, U. Facile Shaping of Flexible MIL-53(Al) for Effective Separation of Propylene over Propane. *Chem. Eng. J.* **2024**, *480*, 147872.

(32) Feng, X.; Qin, M.; Cui, S.; Rode, C. Metal-organic framework MIL-100(Fe) as a Novel Moisture Buffer Material for Energy-efficient Indoor Humidity Control. *Build. Environ.* **2018**, *145*, 234−242.

(33) Shabir, F.; Sultan, M.; Miyazaki, T.; Saha, B. B.; Askalany, A.; Ali, I.; Zhou, Y.; Ahmad, R.; Shamshiri, R. R. Recent Updates on the Adsorption Capacities of Adsorbent-adsorbate Pairs for Heat Transformation Applications. *Renew. Sust. Energy Rev.* **2020**, *119*, 109630.

(34) Grande, A. C.; Águeda, I. V.; Spjelkavik, A.; Blom, R. An Efficient Recipe for Formulation of Metal-organic Frameworks. *Chem. Eng. Sci.* **2015**, *124*, 154−158.

(35) Muttakin, M.; Pal, A.; Rupa, M. J.; Ito, K.; Saha, B. B. A Critical Overview of Adsorption Kinetics for Cooling and Refrigeration Systems. *Adv. Colloid Interface Sci.* **2021**, *294*, 102468.

(36) Alsaman, A. S.; Askalany, A. A.; Harby, K.; Ahmed, M. S. Performance Evaluation of a Solar-driven Adsorption D esalination-cooling system. *Energy* **2017**, *128*, 196−207.

https://doi.org/10.1021/cbe.4c00008
Chem Bio Eng. 2024, 1, 817−825